Boiling-Slurry Reactor: Feasible Operation and Stability

J. Khinast and D. Luss
Dept. of Chemical Engineering, University of Houston, Houston, TX 77204

T. M. Leib
DuPont Engineering, Wilmington, DE 19880

M. P. Harold
DuPont Dacron, Wilmington, DE 19880

In this study the feasible operation and stability of a special boiling-slurry reactor (BSR), in which a single exothermic chemical reaction occurs, are determined. Its feed consists of a nonvolatile liquid reactant dissolved in an inert solvent and gaseous reactants, while the effluent consists only of gaseous components. The BSR attains a unique steady state within a bounded range of operating conditions, the boundaries of which are defined by simple algebraic expressions. While the unique steady states are usually locally stable, they are not always globally stable. For example, when the start-up temperature is too low, the reactor may not reach the steady state and instead reach a "fill-up" state. In that state the liquid volume continuously increases, while the concentrations and temperature remain essentially constant. For some sets of start-up temperatures two distinct fill-up states may exist. When the start-up liquid volume and temperature are very high, a "dry-up" state may exist so that the liquid continuously decreases, while the reactor temperature and concentration remain essentially constant. This state eventually will shift the reactor to the unique steady state. Dry-up, fill-up, and a steady state coexist in some parts of the feasible operation region, thus requiring a special start-up procedure. The BSR may exhibit sustained oscillations for some parameter sets.

Introduction

In a slurry bubble-column reactor gaseous and liquid reactants react on solid-catalyst particles, suspended in a liquid by the gas phase. Slurry reactors are extensively used to carry out highly exothermic reactions such as hydrogenations, oxidations, and halogenations, since they provide excellent temperature control and uniformity. The temperature uniformity often extends the catalyst life and reduces byproduct formation by circumventing the deleterious impact of hot spots prevalent in other types of multiphase reactors such as trickle beds. The suspended catalyst is confined to the reactor and may be periodically or continuously replaced by fresh catalyst. The liquid phase may be stationary when used as an inert medium (semibatch operation), as in liquid-phase methanol synthesis (Cybulski, 1994).

The engineering of these reactors has been reviewed in books by Shah (1979), Ramachandran and Chaudhari (1983), Gianetto and Silveston (1986), Fan (1989), and articles by Hammer et al. (1984), Beenackers and van Swaaij (1986), and Krishna and Ellenberger (1995). When the reactor effluent is a liquid, separation of the suspended catalyst from the effluent is required to reduce catalyst makeup cost and avoid product contamination and toxic-waste production. This separation often requires expensive hardware such as large settlers or hydrocyclones, and may be further complicated by catalyst attrition. The operation and stability of a boiling reactor system has been investigated by several researchers. Luyben (1966) studied the stability of a reactor with a liquid

Correspondence concerning this article should be addressed to D. Luss.

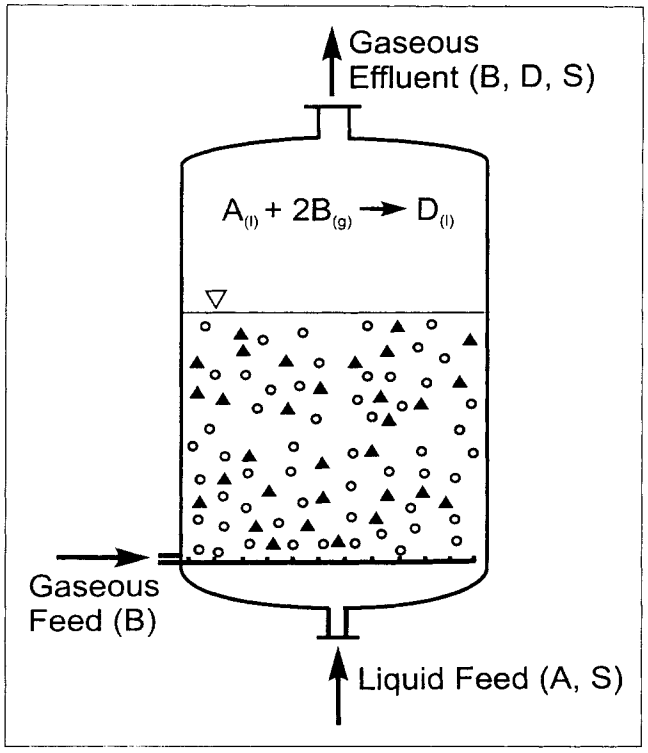

Figure 1. Boiling-slurry reactor.

cooled by evaporation of the reaction mixture. He showed that control may be required for stable operation.

We consider a special configuration of a boiling-slurry reactor. It is fed by a nonvolatile liquid reactant A dissolved in an inert volatile solvent and a gaseous reactant B, while the effluent consists only of gases (Figure 1). Since the liquid reactant is nonvolatile complete conversion of the liquid reactant has to be obtained at a steady state. This configuration has two advantages:

1. The catalyst remains in the reactor, avoiding the need for expensive catalyst/product separation. While internal filtering may be used when catalyst attrition does not occur, in most cases catalyst separation from the product is one of the difficult tasks involved in slurry reactor operation.

2. An inert miscible liquid (solvent) with higher volatility than the liquid reactant may be introduced along with the reactant to cool the reactor and eliminate the need for expensive heat exchangers.

We call this configuration the boiling-slurry reactor (BSR). Potential applications include exothermic gas–liquid reactions for which the reaction products are more volatile than the liquid reactant, for example, the hydrogenation of pyrrole (C_4H_4NH, boiling point 130°C) to pyrrolidine (C_4H_8NH, boiling point 89°C). It should be noted that boiling-liquid reactors have been used in several commercially important processes, such as C_4-alkylation and the synthesis of tetraethyl lead and polyethylene.

Our objectives are to determine the operating conditions for which a BSR operation is feasible and to gain an understanding of its dynamic features. Since complete conversion of the liquid reactant A is obtained, the reactor has at most one steady state. We shall show that even when this unique steady state is linearly stable other pseudo-steady-states with a continuous change of the liquid level may exist for some parameter values and initial conditions. For some parameter values the unique steady state is unstable and an oscillatory state exists.

Mathematical Model of the BSR

We consider a BSR in which an exothermic catalytic gas–liquid reaction

$$A(l) + 2B(g) \rightarrow D(l) \tag{1}$$

occurs. The nonvolatile reactant A is dissolved in an inert volatile solvent S. It has to be completely converted under steady-state conditions to avoid its accumulation in the reactor. The gaseous feed consists of pure B and is dissolved in the liquid phase to react with the liquid reactant A. The heat generated by the exothermic reaction evaporates both the liquid product (D) and the aqueous solvent (S) and preheats the feed. The solid catalyst particles are dispersed in the liquid phase.

Gas mixing in large-diameter slurry reactors is intermediate between plug and well-mixed flow. In most applications the gaseous reactant conversion is small or incomplete so that models assuming either plug- or well-mixed gas flow predict rather similar behavior. The exact description of the gaseous flow pattern is a secondary issue of the problem we consider. Thus, we assume that each phase is perfectly mixed and that the two phases have the same temperature.

A gas–liquid mass-transfer resistance exists only in the liquid phase, while that in the gas phase is negligible. The reaction rate per unit weight of the catalyst can be described by the Langmuir–Hinshelwood relation

$$r = k_0 \exp[-E/RT] \frac{K_{ad} \cdot c_{A,l} c_{B,l}}{1 + K_{ad} c_{A,l}}, \qquad K_{ad} = K_{ad,0} \exp[-\Delta H_{ad}/RT], \tag{2}$$

that is, we ignore any intraparticle diffusional limitations and solid–liquid mass-transfer resistances. The liquid-phase molar balances of the four species A, B, D, and S are

$$\frac{d(c_{i,l} V_l)}{dt} = F_{i,l}^f - \dot{N}_i^t + \nu_i \rho_s V_s r, \qquad i = A, B, D, S, \tag{3}$$

where $F_{i,l}^f$ is the molar feed rate of component i in the liquid. The gas–liquid mass-transfer rates $\dot{N}_i^t$ are

$$\dot{N}_i^t = \begin{cases} 0, & i = A \\ V_l k_l a_v \left[c_{B,l} - \dfrac{p_B}{H_B(T)} \right], & i = B \\ V_l k_l a_v \left[c_{i,l} - \dfrac{c_l y_i}{K_i(T)} \right], & i = D, S, \end{cases} \tag{4}$$

where y_i is the mole fraction of component i in the gas phase, and c_l is the total molar liquid concentration. Finally, the sum of the liquid volume fractions of all the components is unity, that is,

$$c_{A,l}\hat{V}_A + c_{B,l}\hat{V}_B + c_{D,l}\hat{V}_D + c_{S,l}\hat{V}_S = 1, \tag{5}$$

where $\hat{V}_i$ is the partial molar volume of i. The gas-phase mass balances for the three species (B, D, S) are

$$\frac{1}{R}\frac{d[p_i/T\cdot(V_b+V_g)]}{dt} = F^f_{i,g} - F_g\cdot\frac{p_i}{P} + \dot{N}^t_i, \quad i = B, D, S, \tag{6}$$

The overall energy balance is

$$\left(V_l\sum_i c_{i,l}c_{p,i,l} + \frac{(V_g+V_b)}{RT}\sum_i p_i c_{p,i,g} + V_s\rho_s c_{p,s}\right)\frac{dT}{dt} = -\Delta H_r(T)\rho_s V_s r - \sum_i \dot{N}^t_i\cdot\{\Delta H^v_i(T_R) + (c_{p,i,g}-c_{p,i,l})(T-T_R)\} - \sum_i F^f_{i,l}c_{p,i,l}\cdot(T-T^f_l) - \sum_i F^f_{i,g}c_{p,i,g}\cdot\left(T-T^f_g\right), \quad i = A, B, D, S. \tag{7}$$

The effluent gas rate is determined by a PI pressure controller, that is,

$$\frac{d(F_g/c_g)}{dt} = k_P\frac{d(P-\hat{P})}{dt} + \frac{d}{dt}\left[k_I\int_0^t (P(s)-\hat{P})\,ds\right] \tag{8}$$

The bubble phase volume V_b is assumed to follow the Saxena (1995) correlation,

$$\frac{V_b}{V_b+V_l+V_s} = \frac{u_g}{2.5u_g+u^t_b} \tag{9}$$

$$u_g = \frac{F_g}{c_g A_r}. \tag{10}$$

where u^t_b is the terminal rise velocity of the bubble swarm, and u_g the superficial effluent gas velocity. According to Saxena and Chen (1993) u^t_b is a function of the slurry viscosity, surface tension, and the vapor pressure of the liquid. To reduce the number of parameters in the model we assume u^t_b to be a constant (0.23 m/s), which corresponds to the averaged conditions in the reactor. The gas-head volume above the liquid level, V_g, is obtained by subtracting the slurry and bubble phase volume from the reactor volume, i.e.,

$$V_g = V_R - V_l - V_b - V_s. \tag{11}$$

The model equations include 15 dependent variables (four liquid concentrations, $c_{i,l}$; three partial pressures, p_i; and V_l, V_g, V_b, P, c_g, T, F_g, u_g) that are described by nine ODEs, Eqs. 3, 6, 7, 8, and four algebraic equations, Eqs. 5, 9–11. Two additional algebraic relations are the ideal gas law and the sum of all partial pressures being equal to the total pressure. The independent variables are the molar feed rates and temperatures: $F^f_{A,l}$, $F^f_{S,l}$, $F^f_{B,g}$, T^f_l, and T^f_g.

To simplify the analysis and presentation of the results, we reduce the number of parameters by assuming that the Henry's law constant, H_B, does not depend on the temperature. The equilibrium coefficients K_i in Eq. 4 are given by

$$K_i = \frac{P_{v,i}}{P}. \tag{12}$$

Throughout this work we assume that the liquid-feed temperature is equal to the reference temperature $T_R = 298$ K. The parameter values used in the simulations are reported in Table 1. The vapor pressures P_v of the components D and S were computed by the relations

$$\log(P_{v,D}) = 4.791 - 1717.4/T \tag{13}$$

$$\ln(P_{v,S}) = 5.4 + (1-z)^{-1}(-7.765z + 1.458z^{1.5} - 2.776z^3 - 1.233z^6), \quad z = 1 - T/647.3. \tag{14}$$

We define the gas-to-liquid reactant feed ratio (B/A ratio) as

$$\beta = \frac{\nu_A}{\nu_B}\frac{F^f_{B,g}}{F^f_{A,l}} = \frac{1}{2}\frac{F^f_{B,g}}{F^f_{A,l}}. \tag{15}$$

A β value of unity is the minimum required for complete conversion of the nonvolatile reactant A. Clearly, to obtain complete liquid-reactant conversion and to avoid its accumulation, β should exceed unity. Finally, the mole fraction of the reactant in the liquid feed is

$$x = \frac{F^f_{A,l}}{F^f_{A,l}+F^f_{S,l}}. \tag{16}$$

We now determine the steady-state behavior of the BSR and the conditions under which it may be attained, and then we discuss the dynamic features of this reactor.

Table 1. Parameter Values Used in the Simulations

Parameter	Value	Parameter	Value
A_R	1.8 m^2	k_0	$4\cdot10^7$ kmol/(s·kg$_{cat}$)
$c_{p,s}$	1.1 kJ/kg/K	$K_{ad,0}$	0.1 m^3/kmol
$c_{p,A,l}$	150 kJ/kmol/K	k_P	0.1 m^3/bar/s
$c_{p,B,l}$	50 kJ/kmol/K	k_I	0.01 m^3/bar/s^2
$c_{p,D,l}$	150 kJ/kmol/K	$k_l a_v$	0.05 1/s
$c_{p,S,l}$	75 kJ/kmol/K	$\hat{P}$	70 bar
$c_{p,B,g}$	29 kJ/kmol/K	T_R	298.0 K
$c_{p,D,g}$	40 kJ/kmol/K	u^t_b	0.23 m/s
$c_{p,S,g}$	36 kJ/kmol/K	$\hat{V}_A$	0.073 m^3/kmol
E	83 kJ/mol	$\hat{V}_B$	0.01 m^3/kmol
$F^f_{A,l}$	0.075 kmol/s	$\hat{V}_C$	0.081 m^3/kmol
$F^f_{D,l}$, $F^f_{B,l}$	0.0 kmol/s	$\hat{V}_D$	0.018 m^3/kmol
ΔH_{ad}	−21 kJ/mol	V_R	20 m^3
ΔH_r	−251 kJ/mol	V_S	0.8 m^3
$\Delta H^v_D(T_R)$	29 kJ/mol	ν_A	−1
$\Delta H^v_S(T_R)$	44 kJ/mol	ν_B	−2
$\Delta H^v_B(T_R)$	1 kJ/mol	ν_D	+1
H_B	60 m^{3}bar/kmol	ν_S	0
		ρ_s	1,500 kg/m^3

Feasible Steady-State Operation of a BSR

A unique feature of the BSR is that at any steady-state the nonvolatile reactant A is completely converted, since otherwise liquid-phase accumulation occurs. Consequently, at a steady-state the reaction rate and the gas–liquid mass-transfer rates are proportional to the feed rate of A. Since the rate of the heat generation is proportional to the feed rate of the liquid reactant A, it is easily shown that the steady-state temperature depends only on the feed composition and temperatures, that is,

$$T = f\left(x, \beta, T_l^f, T_g^f\right), \tag{17}$$

and not on the system pressure, gas, and liquid holdup, the mass-transfer coefficients, or kinetic parameters. The procedure used to determine the unique steady states is described in the Appendix.

The steady-state reactor temperature and the rate of heat generation increase as the feed concentration of the liquid reactant A increases. However, the reactor temperature decreases with increasing the gas-to-liquid reactant feed ratio (B/A ratio) (Figure 2) as more heat is required to preheat the gas fed to the reactor. Increasing the gas-feed temperature increases the reactor temperature. All the β curves in Figure 2 intersect at a reactor temperature equal to the gas-feed temperature since at this point the excess gas-feed rate does not influence the reactor temperature.

The mole fractions of the three effluent components (B, D, S) also depend only on the feed composition x and β, since complete conversion of A is obtained at a steady state (Appendix):

$$y_i = f(x, \beta), \qquad i = B, D, S. \tag{18}$$

The liquid concentrations in the reactor, however, depend on all the parameters except for the mass-transfer coefficients. We show in the Appendix that the liquid concentration of A satisfies an expression of the form

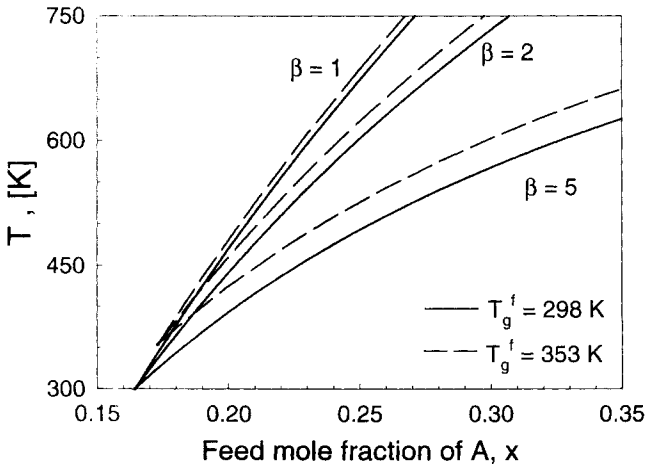

Figure 2. Dependence of the reactor temperature on the liquid reactant feed concentration and the gas-to-liquid reactant feed ratio β.

In both cases $T_l^f = 298$ K.

$$c_{l,A} = \frac{-p + \sqrt{p^2 - 4qs}}{2q}, \tag{19}$$

where p, q, and s are defined by Eq. A23. The remaining steady-state liquid concentrations (S, D, B) and the liquid volume may be computed by substitution of $c_{l,A}$ into the model equations, as described in the Appendix. Note that the model predicts that the mass-transfer coefficient only influences the steady-state liquid volume in the reactor, but not the liquid concentrations. Therefore, at steady state a unique liquid volume corresponds to a specified mass-transfer coefficient.

The BSR may attain a steady state only within a bounded region of operation conditions. Several boundaries of feasible operation can be derived from Eq. 19, such as,

$$p^2 = 4qs, \qquad q = 0. \tag{20}$$

However, stronger feasibility conditions exist. The boundaries of the feasibility region consist of two types. The first depends only on the feed and operation conditions, the second on the reactor and catalyst volume. For example, when the feed rate of the gaseous reactant is smaller than that needed for complete conversion of the nonvolatile reactant A, the liquid level in the reactor will rise continuously and no steady state can be obtained. Thus, one feasibility boundary is $\beta = 1$.

Since the heat generation is proportional to the feed rate of the liquid reactant, it bounds the amount of liquid that can be evaporated. Thus, another boundary of the feasible operation, which we call *heat-generation limit*, bounds cases for which the heat generated by the reaction is not sufficient to boil off the liquid product and the solvent. At this boundary the liquid volume in the reactor is very large (infinite) and, due to the large interfacial area between the gas and liquid ($V_l \cdot a_v$), equilibrium is established between the gas and volatile liquid-phase concentrations. We show in the Appendix that at this boundary

$$\frac{P_{v,D} - p_D}{p_D} - \frac{p_S}{P_{v,S} - p_S} = f[x, \beta, T, P, k(T), K_{ad}(T), H_B, \rho_s, V_s, \ldots], \tag{21}$$

which is a function of the feed conditions and the system parameters. Inspection of Eq. 21 shows that for a wide range of parameters the term on the righthand side is negligible, so that an approximate heat-generation limit is

$$\frac{P_{v,D} - p_D}{p_D} - \frac{p_S}{P_{v,S} - p_S} = 0. \tag{22}$$

The vapor pressures depend only on the temperature, which, in turn, depends only on the feed conditions. Thus, the simplified expression for the heat-generation limit depends only on the feed conditions and the reactor pressure. The exact and simplified feasibility boundaries for three different gas-feed temperatures are compared in Figure 3 in the plane of the reactor temperature T vs. x, the feed mole fraction of A. Note, that the gas-to-liquid-feed ratio β changes

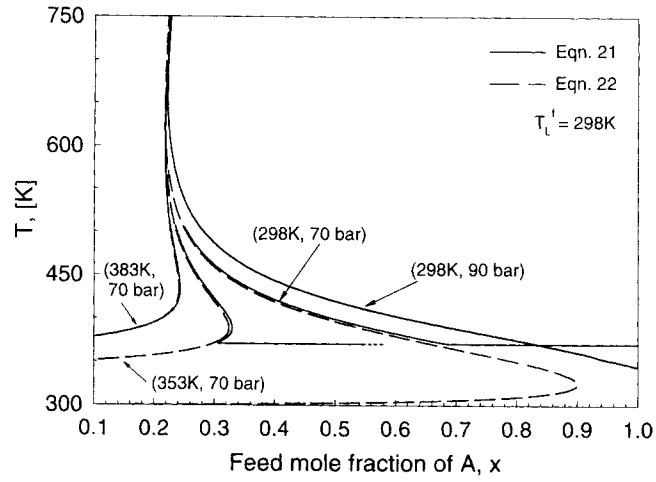

Figure 3. Comparison of the exact (solid lines) and simplified expressions (dashed lines) for the feasibility boundary.

Numbers define gas feed temperature and reactor pressure.

along the curves, since every (T, x)-pair corresponds to a unique β value. Although the exact boundary is the conservative one, the exact and simplified boundaries are almost identical in the region of interest. However, for $T_g^f = 298$ K and $T_g^f = 353$ K the two boundaries deviate below a certain critical reactor temperature. This occurs since below a minimum reactor temperature, $T_{\min}$, steady-state operation is impossible due to kinetic limitations. While the exact boundary predicts this restriction, the simplified one does not. At the minimum temperature the steady-state reaction rate is equal to the feed rate of the liquid reactant:

$$F_{A,l}^f = \rho_s V_s k(T) \frac{K_{ad}(T) c_{A,l} c_{B,l}}{1 + K_{ad}(T) c_{A,l}} \tag{23}$$

Below this temperature this reaction rate cannot be sustained. The highest possible reactant concentrations are $c_{A,l} = 1/\hat{V}_A$ and $c_{B,l} = \hat{P}/H_B$. By inserting these conditions into Eq. 23, a conservative bound on the minimum operation temperature is implicitly defined. In our specific example this relation predicts that $T_{\min} = 368$ K. When the gas-feed temperature exceeds $T_{\min}$, this limit is not encountered, as when $T_g^f = 383$ K in Figure 3, for which the simplified and exact expressions are almost identical. In the parameter region of interest, the simplified expression predicts very accurately the feasibility boundary. While the simplified feasibility boundary, Eq. 22, depends only on the feed conditions, the minimum temperature also depends on the kinetic parameters. Calculations show (see Figure 3) that increasing the reactor pressure shifts the heat-generation limit to higher reactor temperatures for a fixed feed composition, thereby decreasing the region of feasible operation.

Another operation constraint is that the evaporation of the solvent and product should not cause the liquid reactant concentration $[c_{A,l}/(c_{A,l} + c_{S,l})]$ to exceed its *solubility limit* (assumed to be 0.5 in our example). This solubility limit is a curve in the plane of the feed conditions (β vs. x). Any operation beyond this boundary leads to a separation between the nonvolatile reactant A and the solvent S. While the mathematical model used here does not account for such phase separation, it may occur in specific applications.

The feasibility boundaries described earlier depend only on the composition and temperature of the feed and the stoichiometry of the reaction. There are two additional boundaries that are determined by the reactor and catalyst volume. The first is the *full reactor* boundary, which is the set of parameters for which the expanded slurry volume (liquid, bubbles, and catalyst) is equal to that of the total reactor volume. Operation beyond this limit leads to a spillover of the reactor contents and requires either a shutdown or an adjustment of the operating conditions.

The BSR has to be operated so that all the catalyst is immersed in the liquid. Thus, another feasible design boundary is the *catalyst wetting limit* at which any further reduction of the liquid volume dries some of the catalyst. We assumed that this occurs when $V_l = V_s$. Note that in some specific applications it may be feasible to operate beyond this boundary. The model presented here does not account for this mode of operation, and we assume that the reactor will be either shut down or the operation conditions will be adjusted if this limit is reached.

The five feasibility boundaries, shown in Figure 4 in the β vs. x plane, bound a region in which a steady-state operation is feasible. Steady-state operation below the $\beta = 1$ curve is not feasible, as there is not enough gaseous reactant feed to convert all of the liquid reactant A. Operation to the left of the heat-generation limit is not feasible, as continuous liquid accumulation will fill the BSR and cause a spillover. Operation to the right of the solubility limit will lead to phase separation between the reactant and its solvent. Operation below the full reactor boundary will lead to spillover, while operation above the catalyst wetting limit will leave some of the catalyst dry. (The full reactor limit eventually bends and becomes very close to the heat-generation limit, so that both cannot be distinguished in the figure.) *A-priori* construction of the various boundaries reduces significantly the experimental effort needed to determine operating conditions for which steady-state operation may be attained.

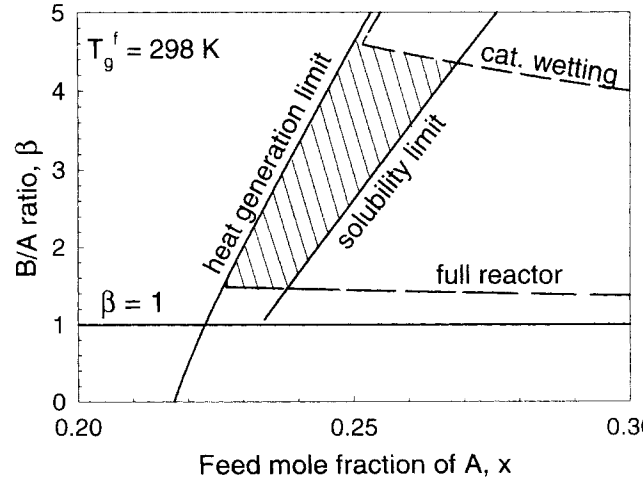

Figure 4. Feasibility map showing regions of feasible steady-state operation (dashed region) of a BSR.

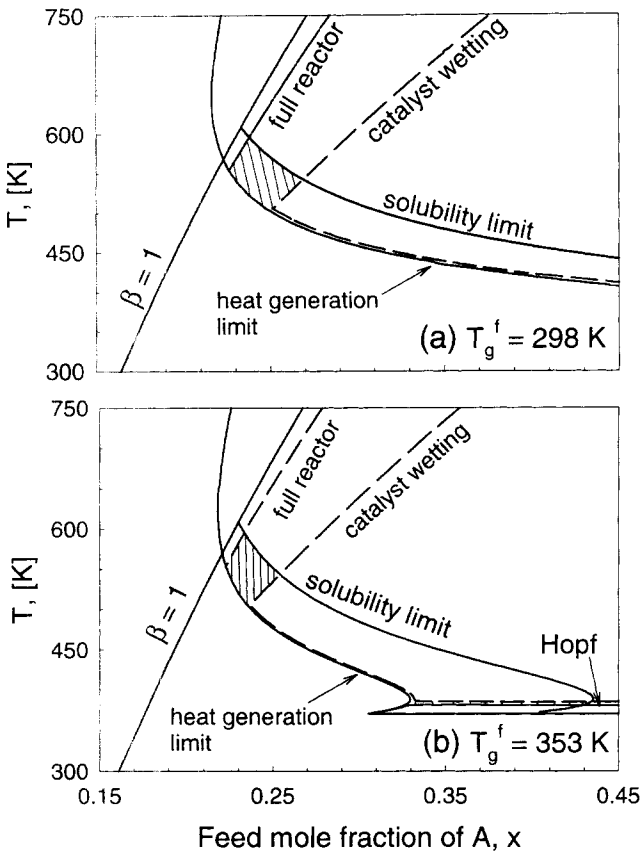

Figure 5. Set of feasibility boundaries in the *T*- vs. *x*-plane for two different gas-feed temperatures.

The region of feasible operation is dashed. Each point in the plane corresponds to a unique pair of β and x.

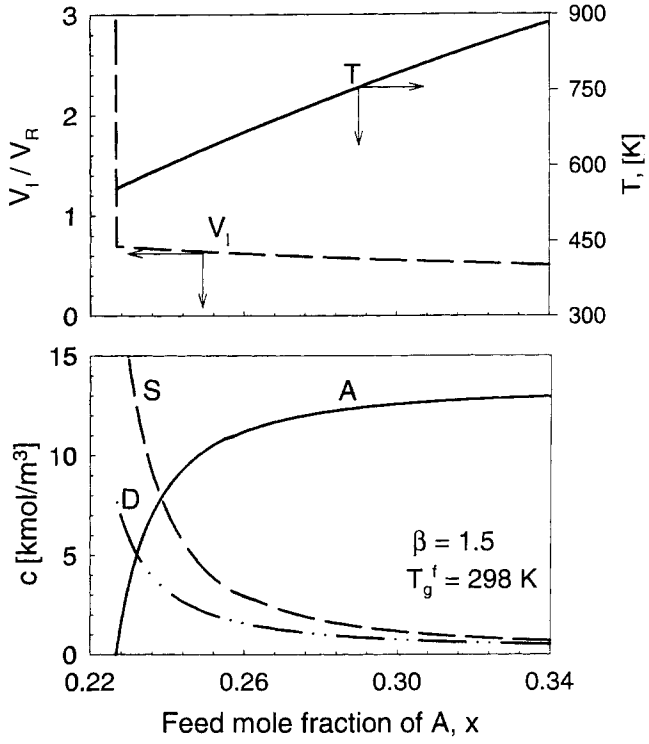

Figure 6. Dependence of the steady-state reactor temperature, liquid volume, and liquid concentrations on the feed mole fraction of reactant *A*.

The heat generation limit is at $x = 0.227$.

A unique steady-state temperature corresponds to any set of β and x values. Thus, the feasibility boundaries may be plotted in the reactor temperature vs. x plane for any specified T_g^f. Two typical plots of the feasibility boundaries are shown in Figure 5. In the dashed region the steady states are feasible and stable and neither oscillations nor temperature excursions will occur. Figure 5 shows that an increase in the gas-feed temperature shifts the feasible operation region to lower reactant feed mole fraction and temperatures. The range of feasible x values is (0.22, 0.255) for $T_g^f = 353$ K and (0.225, 0.27) for $T_g^f = 298$ K.

Figure 6 describes the steady-state variables as the heat-generation limit is approached. At a critical feed reactant mole fraction (heat-generation limit) the steady-state liquid volume suddenly increases without bounds. The liquid consists mainly of the solvent S and the product D, which do not evaporate at low temperatures, thus leading to an increase in their concentrations. While the feed is consumed at the steady state, the concentration of A decreases due to the increased liquid volume.

Dynamics of the BSR

The BSR has a unique steady-state solution for all operating conditions within the feasible region. Linearization and numerical simulations showed that in our example these unique steady states are locally stable for all practical sets of operating conditions. However, the steady-state solutions may be destabilized for extreme (and unpractical) choice of parameter values. Figure 5 shows that a Hopf bifurcation exists for $T_g^f = 353$ K for very large B/A ratios ($\beta > 20$) and large x. In this case the unique steady-state is unstable and the model predicts oscillatory states as shown in Figure 7. (Note that the predicted liquid volume exceeds the reactor volume.) Changes in the proportional and integral constants did not shift the Hopf bifurcation line, indicating that the PI pressure controller did not cause these oscillations.

Our simulations revealed that in certain cases the BSR exhibits a rather surprising dynamic behavior when the unique steady state is locally stable. Specifically, for certain conditions the slurry volume continuously increases, that is, $dV_l/dt > 0$, while the concentrations of all the species and the reactor temperature remain essentially unchanged. We refer to this pseudo-steady-state as the *fill-up state*. When the liquid volume in the reactor volume is very large, an inverse behavior of a *dry-up state* may be obtained, that is, $dV_l/dt < 0$, in which the liquid volume continuously decreases, while the reactor temperature and concentrations are essentially constant. While the fill-up state does not change with time (as long as the reactor does not fill up leading to spillover), the dry-up state eventually breaks down as the liquid volume decreases and converges to the unique steady state.

The fill-up and dry-up states may be predicted by a limiting model that exploits the fact that the liquid volume, and hence also the bubble phase volume, have a much larger time

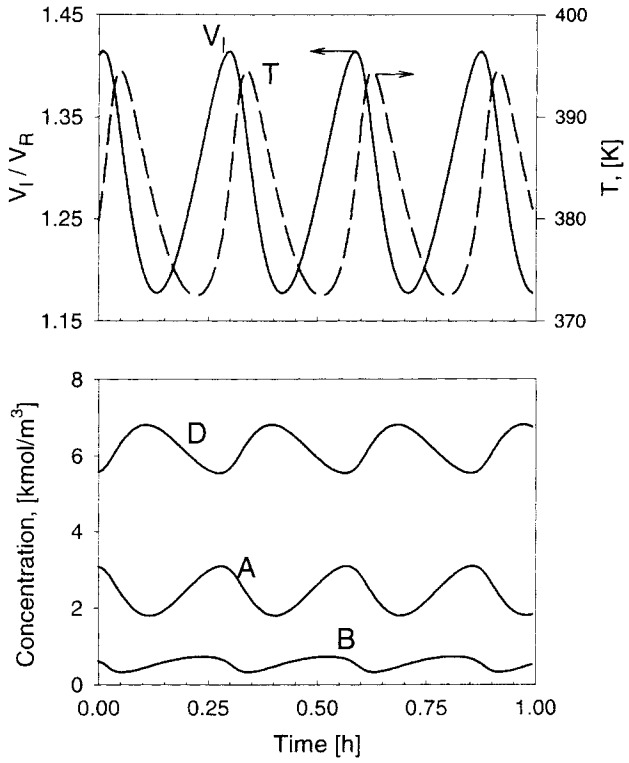

Figure 7. Time series of the reactor temperature, liquid volume, and liquid concentrations of an oscillatory state obtained for $\beta = 85$, $x = 0.34$, and $T_g^f = 353$ K.

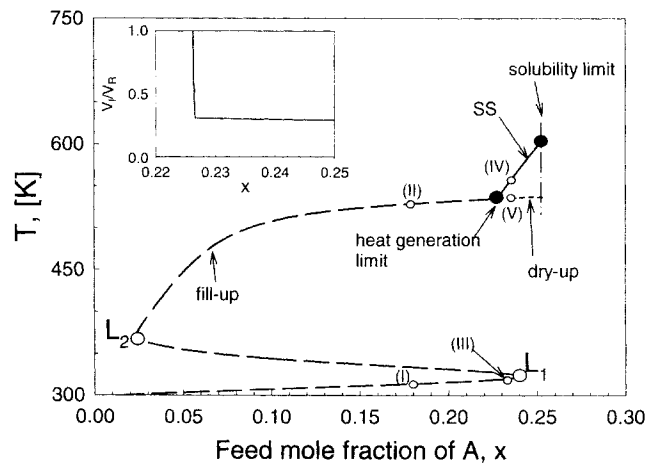

Figure 8. Bifurcation diagram of the feasible steady states (solid line), fill-up states (dashed line), and dry-up states (short dashed line) as a function of the feed mole fraction of the limiting reactant *A* for $\beta = 2.5$ and $T_g^f = 353$ K.

L = limit point; SS = steady state. The inset is the steady-state liquid volume corresponding to the SS line.

constant than the other state variables and that the temperature and concentrations approach asymptotically constant values during fill-up and dry-up. Thus, these two pseudo-steady-states may be computed by a limiting pseudo-steady-state model, which assumes that the temperature and concentrations remain unchanged during these two pseudo-steady-states. The limiting model is described in the Appendix.

The interaction between the stable steady-state and the two pseudo-steady-states may be illustrated by a bifurcation diagram combining solutions of the full and limiting model. Figure 8 describes the dependence of the steady states (SS, solid lines), fill-up states (long dashed lines), and dry-up states (short dashed lines) on the mole fraction of the limiting reactant A in the feed. The branch of the fill-up states has an ignition point L_1 and an extinction point L_2. A bounded range of feed concentrations exists for which the model predicts three different fill-up states. While either low- and high-temperature fill-up states may be attained, no state on the intermediate branch of the unstable fill-up states (bounded between L_1 and L_2) can be reached. Eventually, the branch of reactor fill-up states touches the steady-state branch. At this point $dV_l/dt = 0$, and it is the heat-generation limit associated with an infinite liquid volume. (The steady-state liquid volume is shown in the small inset in Figure 8.) The continuation of the fill-up branch beyond that point is the branch of dry-up states. Beyond the solubility limit dry-up states cannot be obtained since phase separation would occur.

As seen from Figure 8 a stable fill-up state coexists with the stable steady state and dry-up state for a bounded range of the feed mole fraction of the limiting reactant A. The existence of fill-up states outside the feasible steady-state operation region is mainly of academic interest, as one would not operate a reactor under these conditions. Figure 9 illustrates the shift of the reactor to two different fill-up states following two different initial reactor temperatures. The feed molar fraction of A in this case is smaller than that of the heat-generation limit so that no steady state can exist for these operating conditions. The state corresponding to the lower initial temperature (I in Figure 9) leads to a much more rapid fill-up than state II, obtained for a higher initial temperature. The calculations show that at the higher reactor temperature the reactor fill-up rate is significantly slower since more solvent and reaction product are evaporated (Figure 9). Figure 10 illustrates a case where the feed molar fraction of A is between the heat-generation and solubility limits, so that a steady state can be obtained for these operating conditions. When the initial reactor temperature is $T = 313$ K, the fill-up state (shown as III in Figure 10) is established rapidly. We note that after a short while (~ 0.5 h) the slurry volume becomes very large, leading to spillover and requiring reactor shutdown. Starting at a higher initial temperature, $T = 373$ K, the reactor shifts smoothly to the steady-state (case IV). If the operation is started with a very large liquid volume (case V) and $T = 515$ K, the liquid volume slightly increases initially and shifts to the dry-up state, that is, the slurry volume continuously decreases but the reactor temperature remains constant (532 K). The liquid volume decreases for about 5 h and then shifts to the unique steady state ($T = 555$ K). The preceding simulations show that even though a unique state is usually stable, the reactor may not converge to it if started up at too low a temperature. The liquid volume has by far the largest time constant in the system. Thus, in order to converge as fast as possible to the steady state, it is useful to

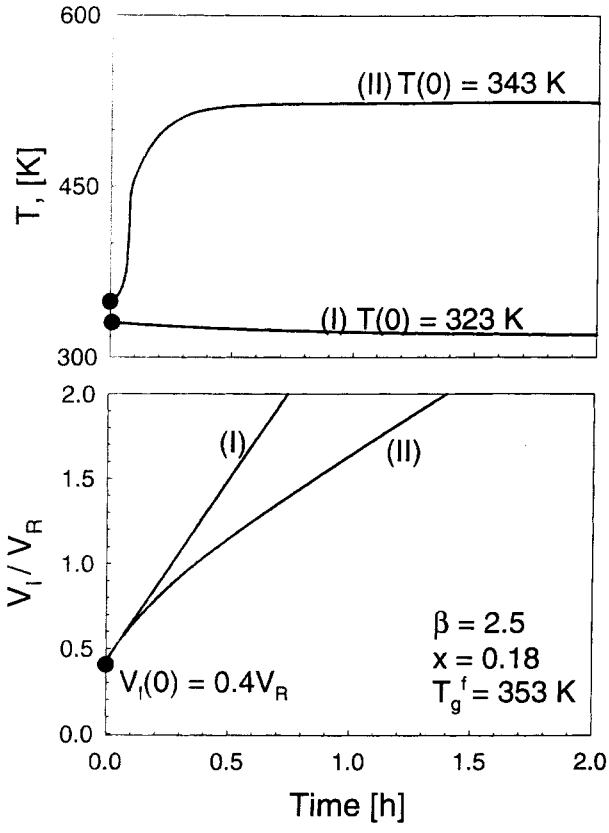

Figure 9. Shift of the BSR to different fill-up states for two initial reactor temperatures for operating conditions without steady state.

Roman numerals refer to states marked in Figure 8.

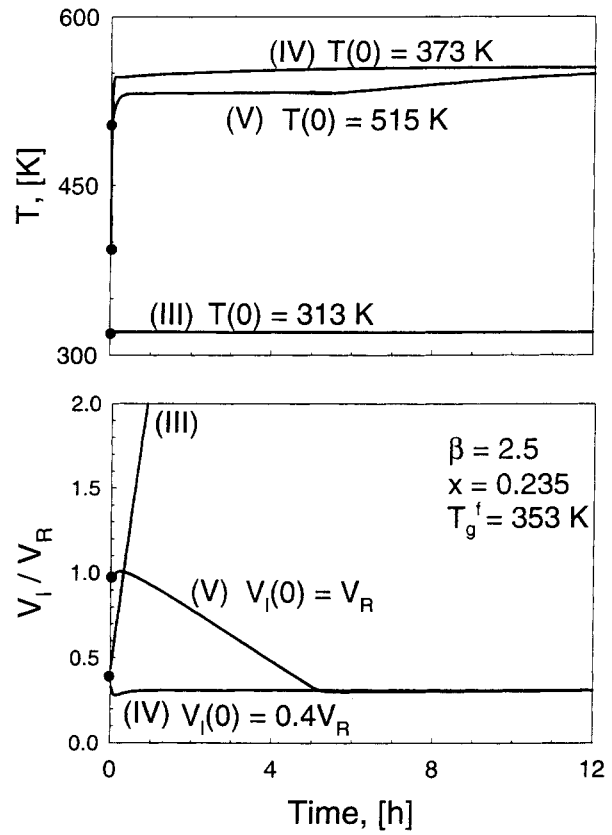

Figure 10. Dynamic behavior of the BSR for three different initial reactor temperatures for a case where a steady-state, fill-up, and a dry-up state coexist.

Roman numerals refer to states marked in Figure 8.

start the operation with a slurry volume close to that of the steady state and a startup temperature equal to that of the steady state.

The preceding analysis indicates that within the feasible region undesired reactor behavior (fill-up or dry-out) may occur only for feed conditions bounded between the ignition limit point L_1 of the branch of fill-up states and the heat-generation limit (see Figure 8). Both fill-up and dry-up states will require eventual shutdown unless the operating conditions are adjusted, such as by an increase of the gas-feed temperature. It is important to determine the location of L_1 within the feasible region in order to check if the choice of the initial start-up temperature may lead to a fill-up or dry-up state.

Figure 11 shows the loci of the heat-generation limit, the solubility limit, and the limit point L_1 (see Figure 8), computed by the method described by Khinast et al. (1998), for two gas-feed temperatures of 353 K and 383 K. In a region below the L_1 line, a shift to a fill-up state is possible. While the change in feed temperature has only a moderate impact on the location of the heat-generation line, it changes appreciably the position of the L_1 curves. Inspection of Figure 11 shows that for a gas-feed temperature of 383 K the unique steady state will be attained for all initial conditions for essentially all values of x and β, except those in a very small region (*cdef*), bounded by L_1, the solubility limit, $\beta = 1$, and the heat generation limit. However, for a lower feed temperature of 353 K a much larger region (*CDEF*) in the x and β plane exists in which a low start-up temperature will lead to a fill-up instead of the steady state.

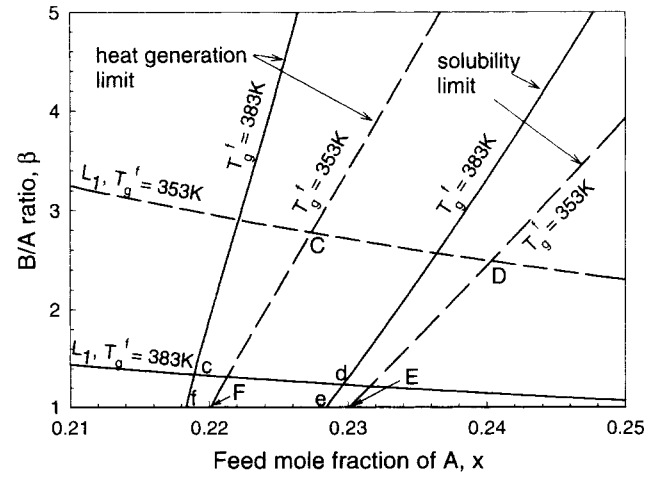

Figure 11. Dependence of the heat-generation limit, solubility limit, and L_1 on β and x for two different gas feed temperatures.

In the region *CDEF* and *cdef* fill-up states may be obtained if operating conditions are not adjusted.

The common independent (input) variables are x, β, and the feed temperatures. In general, the reactor is operated such that the liquid level and the temperature in the reactor should be close or equal to a given set point. We consider the case that only the feed rate and feed temperature of the gas may be adjusted to maintain the reactor at preselected temperatures and slurry holdup. Figure 12 shows the required values of β and T_g^f in response to changes in the liquid reactant feed mole fraction x in order to keep the reactor at three different set points: $T = 600$ K and $\epsilon_{sl} = 0.7$, $T = 600$ K and $\epsilon_{sl} = 0.8$, $T = 625$ K and $\epsilon_{sl} = 0.8$, where ϵ_{sl} is the hold-up of the expanded slurry phase

$$\epsilon_{sl} = \frac{V_l + V_s + V_b}{V_R}. \tag{24}$$

We note that the required adjustment in the β values as the feed mole fraction of A is changed is rather small, whereas those of the gas-feed temperatures are large. Obviously, the reactor can be operated only in a range of $x = 0.2$–0.24, since otherwise the required gas-feed temperature would be too high or too low. A change in the slurry holdup set point requires mainly an adjustment of the β values, whereas a change in the reactor temperature set point requires mainly an adjustment of the gas-feed temperature. We conclude that the gas-feed temperature enables control of the reactor temperature, whereas the gas-feed rate influences mainly the liquid level in the reactor.

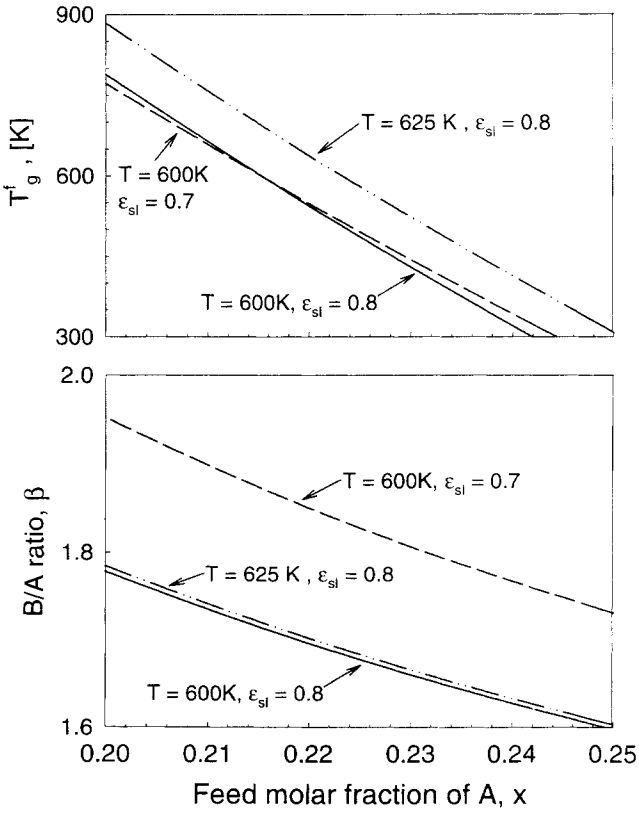

Figure 12. Values of T_g^f and β needed to keep the reactor at three different set point values of the slurry holdup and temperature.

Conclusions and Remarks

The BSR has two major advantages over usual slurry reactor operation. It avoids the need to separate the effluent and the catalyst, and the addition of a suitable solvent enables a convenient temperature control of the exothermic reaction. The BSR configuration considered by us attains a steady state only within a bounded region of operating conditions. This region is bounded by several constraints in the parameter space. Some of these constraints depend only on the specific feed and operating conditions, that is, the stoichiometric requirement for complete conversion of the nonvolatile reactant, the heat required to evaporate the product and solvent and to preheat the feed, and the need to keep the limiting liquid reactant in the solution. Two additional constraints are due to the reactor and catalyst volume. One is that the slurry volume cannot exceed the reactor volume, the second is that the catalyst needs to be wet. A shift to the feasible operating region may be accomplished by adjusting various operating conditions such as the gas-feed temperature and flow rate, liquid-feed temperature, concentration, and flow rate, as well as the reactor pressure.

The BSR steady-state temperature depends exclusively on the feed conditions (mole fraction of A in the liquid feed, B/A ratio, gas and liquid temperatures) and thermodynamic properties. The liquid- and gas-feed rates, kinetic and mass-transfer parameters, total pressure, and liquid and bubble holdup do not influence that temperature. The steady-state composition of the effluent depends solely on the feed composition. While the liquid concentrations depend on the full parameter set except for the mass-transfer coefficient, the liquid volume depends on all the parameters. It is inversely proportional to the mass-transfer coefficient and proportional to the liquid-reactant feed rate.

One of the surprising findings of this study was that the unique steady state of the BSR may not be globally stable, even when it is linearly stable. Specifically, when the reactor start-up temperature is sufficiently low, a fill-up state may be obtained, which will require an eventual shutdown to avoid spillover or an adjustment in the operating condition. Similarly, a dry-up state may lead to an extended period of undesired transient operation. The existence of these fill-up and dry-up states and their regions of attraction need to be taken into consideration to enable a rational design of the reactor operation, start-up, and control. Our simulations indicate that for some sets of parameters either two fill-up states or a fill-up, a dry-up, and a steady state may coexist at the same operating conditions. It is worth noting that an experimental observation of fill-up and dry-up states was reported by Hancock and Kenney (1977) for the isothermal reaction between gaseous methanol and HCl in the presence of a concentrated aqueous solution of zinc chloride. While their reaction system and reactor differ from ours, their article underscores the pitfalls that need to be avoided in the start-up of this reactor.

Notation

A_R = reactor cross-sectional area, m^2
c_p = heat capacity, kJ/(kmol·K)
E = activation energy, kJ/kmol
$F^f_{g,i}$ = molar gaseous feed rate of component i, kmol/s
F_g = molar effluent rate of gas phase, kmol/s

ΔH_r = heat of reaction, kJ/kmol
ΔH_{ad} = heat of adsorption, kJ/kmol
ΔH^v = heat of evaporation at T_R, kJ/kmol
K_{ad} = adsorption constant of component A, m^3/kmol
$k_l \cdot a_v$ = volumetric mass-transfer coefficient, 1/s
k_0 = frequency factor, m^3/(s·kg$_{cat}$)
k_I = integral control constant, m^3/(bar·s^2)
k_P = proportional control constant, m^3/(bar·s)
P = system pressure, bar
$\hat{P}$ = desired system pressure, bar
R = universal gas constant
t = time, s
T = reactor temperature, K
V_R = reactor volume, m^3
ν = stoichiometric coefficient
ρ_s = density of solid catalyst, kg/m^3

Superscripts

v = vaporization

Literature Cited

Beenackers, A. A. C. M., and W. P. H. van Swaaij, "Chemical Reactor Design and Technology," Nato Advanced Study Institute Series, H. I. DeLasa, ed., Martinus Nijhoff, Boston, p. 463 (1986).

Cybulski, A., "Liquid-Phase Methanol Synthesis: Catalysts, Mechanism, Kinetics, Chemical Equilibria, Vapor-Liquid Equilibria, and Modeling—A Review," *Catal. Rev.-Sci. Eng.*, **36**(4), 557 (1994).

Fan, L. S., *Gas-Liquid-Solid Fluidization Engineering*, Butterworths, Boston (1989).

Gianetto, A., and O. L. Silveston, *Multiphase Chemical Reactors*, Hemisphere, Washington, DC (1986).

Hammer, H., U. Kusters, H. J. Schrag, A. Soemarno, U. Sahabi, H. Schonau, and U. Napp, *Recent Advances in the Engineering Analysis of Chemically Reacting Systems*, L. K. Doraiswamy, ed., Wiley India, New Delhi, p. 379 (1984).

Hancock, M. D., and C. N. Kenney, "The Stability of a Gas-Liquid Reactor," *Chem. Eng. Sci.*, **32**, 629 (1977).

Khinast, J., D. Luss, M. P. Harold, J. J. Ostermaier, and R. McGill, "Continuously-Stirred Decanting Reactor—Operability and Stability Considerations," *AIChE J.*, **44**(2), 373 (1998).

Krishna, R., and J. Ellenberger, "A Unified Approach to the Scale-Up of 'Fluidized' Multiphase Reactors," *Trans. Inst. Chem. Eng.*, **73**(A), 217 (1995).

Luyben, W. L., "Stability of Autorefrigerated Chemical Reactors," *AIChE J.*, **12**(4), 662 (1966).

Ramachandran, P. A., and R. V. Chaudhari, *Three Phase Catalytic Reactors*, Gordon & Breach, New York (1983).

Saxena, S. C., and Z. D. Chen, "Hydrodynamics of Similarly Baffled Slurry Columns," *Proc. Indus. Chem. Eng. Technol. Topical Conf.*, St. Louis, MO (1993).

Saxena, S. C., "Bubble Column Reactors and Fischer-Tropsch Synthesis," *Catal. Rev.-Sci. Eng.*, **37**(2), 227 (1995).

Shah, Y. T., *Gas-Liquid-Solid Reactor Design*, McGraw-Hill, New York (1979).

Appendix

Derivation of the steady-state variables

At a steady state complete conversion of the liquid reactant is obtained. Therefore, the reaction rate equals the feed rate and the various steady-state gas–liquid mass-transfer rates are proportional to the feed rate of A, that is,

$$\dot{N}_B^t = -2F_{A,l}^f \tag{A1}$$

$$\dot{N}_D^t = F_{A,l}^f \tag{A2}$$

$$\dot{N}_S^t = \left(\frac{1-x}{x}\right) F_{A,l}^f. \tag{A3}$$

Introducing these relations into the energy balance Eq. 7 gives

$$\Delta T = \frac{-\Delta H_r + 2\Delta H_B^v - \Delta H_D^v - \frac{1-x}{x}\Delta H_S^v - \left(c_{p,A,l} + \frac{1-x}{x}c_{p,S,l}\right)\left(T_R - T_l^f\right) - 2\beta c_{p,B,g}\left(T_R - T_g^f\right)}{\frac{x}{1-x}c_{p,A,l} - 2\delta c_{p,B} + \delta c_{p,D} + \frac{1-x}{x}c_{p,S,g} + 2\beta c_{p,B,g}}, \tag{A4}$$

where

$$T = T_R + \Delta T, \qquad \delta c_{p,i} = c_{p,i,g} - c_{p,i,l}. \tag{A5}$$

Hence, except for thermodynamic properties, the reactor temperature depends only on x and β and the feed temperatures. The mole fractions of the three effluent components depend only on the feed composition, x and β. For example, the effluent rate of the gaseous reactant is equal to the feed rate minus its consumption by the reaction, that is,

$$2F_A^f(\beta - 1) = \frac{p_B}{P}F_A^f\left(\frac{1-x}{x} + 1 + 2(\beta - 1)\right). \tag{A6}$$

This may be rewritten as

$$y_B = \frac{p_B}{P} = \frac{2(\beta - 1)}{(1-x)/x + 1 + 2(\beta - 1)}. \tag{A7}$$

Equivalently, we get

$$y_D = \frac{p_D}{P} = \frac{1}{(1-x)/x + 1 + 2(\beta - 1)} \tag{A8}$$

$$y_S = \frac{p_S}{P} = \frac{(1-x)/x}{(1-x)/x + 1 + 2(\beta - 1)}. \tag{A9}$$

The liquid concentrations may be obtained by combining Eqs. 4, A1–A3, and $K_i = P_{v,i}/P$. The liquid concentrations of D and S are related to that of B, that is,

$$\left[c_{D,l} - \frac{c_l p_D}{P_{v,D}}\right] = -\frac{1}{2}\left[c_{B,l} - \frac{p_B}{H_B}\right] \tag{A10}$$

$$\left[C_{S,l} - \frac{c_l p_S}{P_{v,s}}\right] = -\frac{1}{2}\frac{1-x}{x}\left[c_{B,l} - \frac{p_B}{H_B}\right]. \tag{A11}$$

Since

$$c_l = c_{A,l} + c_{B,l} + c_{D,l} + c_{S,l}, \tag{A12}$$

we get

$$c_{D,l} = \frac{1}{f}(\epsilon_1 c_{A,l} + \epsilon_2 c_{B,l} + \epsilon_3),$$

$$c_{S,l} = \frac{1}{f}(\hat{\epsilon}_1 c_{A,l} + \hat{\epsilon}_2 c_{B,l} + \hat{\epsilon}_3), \tag{A13}$$

where

$$\hat{\epsilon}_1 = \frac{P_{v,D}}{P_{v,D} - p_D}, \quad \hat{\epsilon}_2 = \frac{1}{2}\frac{P_{v,D}}{P_{v,D} - p_D} - \frac{1}{2}\frac{1-x}{x}\frac{P_{v,S}}{p_S}, \tag{A14}$$

$$\hat{\epsilon}_3 = \frac{1}{2}\left(\frac{1-x}{x}\frac{P_{v,S}}{p_S} + \frac{P_{v,D}}{P_{v,D} - p_D}\right)\frac{p_B}{H_B} \tag{A15}$$

$$\epsilon_1 = (\hat{\epsilon}_1 + 1)\frac{p_D}{P_{v,D} - p_D}, \quad \epsilon_2 = \hat{\epsilon}_2\frac{p_D}{P_{v,D} - p_D} + \frac{2p_D - P_{v,D}}{2P_{v,D} - 2p_D} \tag{A16}$$

$$\varepsilon_3 = \frac{p_D}{P_{v,D} - p_D}\hat{\varepsilon}_3 + \frac{1}{2}\frac{P_{v,D}}{P_{v,D} - p_D}\frac{p_B}{H_B} \tag{A17}$$

$$f = \frac{P_{v,S} - p_S}{p_S} - \frac{p_D}{P_{v,D} - p_D}. \tag{A18}$$

Combining Eqs. A13 and 5 yields

$$\left(\hat{V}_A + \hat{V}_D\hat{\epsilon}_1 + \hat{V}_S\epsilon_1\right)c_{A,l} + \left(\hat{V}_B + \hat{V}_D\hat{\epsilon}_2 + \hat{V}_S\epsilon_2\right)c_{B,l} = 1 - \hat{V}_D\hat{\epsilon}_3 - \hat{V}_S\epsilon_3, \tag{A19}$$

which may be written as

$$\sigma c_{A,l} + \omega c_{B,l} = \varphi, \tag{A20}$$

with

$$\sigma = \left(\hat{V}_A + \hat{V}_D\hat{\epsilon}_1 + \hat{V}_S\epsilon_1\right), \quad \omega = \left(\hat{V}_B + \hat{V}_D\hat{\epsilon}_2 + \hat{V}_S\epsilon_2\right),$$

$$\varphi = 1 - \hat{V}_D\hat{\epsilon}_3 - \hat{V}_S\epsilon_3. \tag{A21}$$

Inserting Eq. A20 into the reaction-rate expression, Eq. 2, with $r = F^f_{A,l}/(\rho_S V_s)$, and solving for c_A gives

$$c_{A,l} = \frac{-p + \sqrt{p^2 - 4qs}}{2q}, \tag{A22}$$

where

$$p = F^f_{l,A}\omega K_{\text{ad}} - \varphi\mu, \quad q = \sigma\mu, \quad s = \omega F^f_{l,A},$$

$$\mu(T) = K_{\text{ad}}(T)\rho_s V_s k(T). \tag{A23}$$

The remaining liquid concentrations may be computed by substitution of $c_{l,A}$ into Eqs. A13 and A20. The liquid volume may be calculated by inserting the liquid concentrations in Eqs. 4 and A1–A3.

Heat-generation limit

The heat-generation limit bounds operation conditions for which the heat generated by the reaction is not sufficient to boil off the solvent and the liquid product. As this heat-generation limit is approached, the decrease in the rate of heat generation causes the reactor temperature to decrease. This, in turn, reduces the gas–liquid mass-transfer driving force. Hence, to evaporate the liquid product and solvent the interfacial area ($V_l \cdot a_v$) has to increase, which requires a corresponding increase in the slurry volume. The net effect is that as the heat-generation limit is approached, the liquid volume V_l increases. At the heat-generation limit, the mass-transfer driving force becomes negligible while the liquid volume becomes unbounded. This state cannot be attained in any finite-volume reactor, as the spillover attained in a finite-volume reactor will terminate the operation before this limit is reached. Clearly, the heat-generation limit is an upper bound on the feasibility region. At the heat-generation limit, gas–liquid equilibrium is established:

$$c^*_{D,l} = c^*_l\frac{y_D}{K_D(T)}, \quad c^*_{S,l} = c^*_l\frac{y_S}{K_S(T)}, \quad c^*_{B,l} = \frac{p_B}{H_B},$$

$$c^*_l = c^*_{A,l} + c^*_{B,l} + c^*_{D,l} + c^*_{S,l}, \tag{A24}$$

where the * denotes equilibrium concentrations. At a steady-state the feed rate of the liquid nonvolatile reactant has to equal the reaction rate, that is, $r = F^f_{A,l}/(\rho_S V_s)$, the concentration of the reactant needed to maintain a steady state can be determined from Eq. 2, that is,

$$c_{A,l} = \frac{F^f_A}{K_{\text{ad}}(T)\cdot[\rho_S V_S k(T) p_B/H_B - F^f_A]}. \tag{A25}$$

By inserting Eqs. A24 and A25 into Eq. 5, an analytic expression for the heat-generation limit is obtained, which depends only on the feed conditions and system parameters:

$$\frac{P_{v,D} - p_D}{p_D} - \frac{p_S}{P_{v,S} - p_S} = \frac{p_B/H_B + c_{A,l}}{1 - p_B/H_B\hat{V}_B - c_{A,l}\hat{V}_A} \cdot \frac{P_{v,S}}{P_{v,S} - p_S}\left(\hat{V}_D + \frac{1-x}{x}\hat{V}_S\frac{P_{v,D}}{P_{v,S}}\right). \tag{A26}$$

Limiting model

The reactor temperature and the concentrations approach asymptotically constant values during the reactor fill-up or dry-up states. The remaining variables (temperature and concentrations) remain essentially unchanged and may be computed by using a *limiting model*. This model is derived by assuming a large liquid volume ($V_l \gg 0$) and a constant rate of increase in the liquid volume ($dV_l/dt = \dot{V}_l = \text{const.}$). Under these conditions, equilibrium between the gas and liquid phases exists. Therefore, combined liquid–gas phase mass balances may be set up, that is,

$$F_{A,l}^f - \rho_s V_s r = \dot{V}_l c_{A,l} \tag{A27}$$

$$F_{B,g}^l - 2\rho_s V_s r = \dot{V}_l c_{B,l} + \dot{V}_b \frac{p_B}{RT} + F_g \frac{p_B}{\hat{P}} \tag{A28}$$

$$\rho_s V_s r = \dot{V}_l c_{D,l} + \dot{V}_b \frac{p_D}{RT} + F_g \frac{p_D}{\hat{P}} \tag{A29}$$

$$F_{S,l}^f = \dot{V}_l c_{S,l} + \dot{V}_b \frac{p_S}{RT} + F_g \frac{p_s}{\hat{P}}. \tag{A30}$$

Due to the equilibrium, we have

$$p_B = H_B c_{B,l}, \qquad p_D = P_{v,D} c_{D,l}/c_l,$$
$$p_S = P_{v,S} c_{S,l}/c_l. \tag{A31}$$

The energy balance is

$$\sum_i F_{i,l}^f c_{p,i,l} \cdot (T_l^f - T_R) + \sum_i F_{i,g}^f \left[\Delta H_i^v(T_R) + c_{p,i,g} \cdot \left(T_g^f - T_R\right)\right]$$
$$- \Delta H_r(T) \rho_s V_s r = \dot{V}_1 \sum_i c_{i,l} c_{p,i,l} (T - T_R)$$
$$+ \dot{V}_b \sum_i \frac{p_i}{RT} [\Delta H_i^v(T_R) + c_{p,i,g}(T - T_R)] + \tag{A32}$$
$$+ \sum_i F_g \frac{p_i}{P} [\Delta H_i^v(T_R) + c_{p,i,g}(T - T_R)] \qquad i = A, B, D, S.$$

An additional required relation is that the sum of the partial-liquid volumes is unity, Eq. 5. Furthermore, the sum of the partial pressures equals the total pressure, and the changes in the bubble and liquid volumes satisfy the relation

$$\dot{V}_b = \frac{u_g}{1.5u_g + u_b^t} \dot{V}_l, \tag{A33}$$

which was obtained by differentiation of Eq. 9. The limiting model has eight variables ($c_{A,l}$, $c_{B,l}$, $c_{D,l}$, $c_{S,l}$, F_g, T, $\dot{V}_l$, $\dot{V}_g$) and is described by the eight equations just given.

Manuscript received Mar. 24, 1998, and revision received May 29, 1998.